



High-accuracy electrohydraulic control system for the position and orientation of the primary mirror for a large telescope

Yu-Xia Li¹ · Jian-Li Wang¹ · Peng-Fei Guo¹ · Hong-Wen Li¹ · Yu-Yan Cao¹

Received: 10 March 2021 / Revised: 22 June 2021 / Accepted: 23 June 2021 / Published online: 27 August 2021
© The Korean Physical Society 2021

Abstract

Due to variations in gravity, temperature, and external disturbances, the optical axes of a telescope's primary mirrors can shift and, consequently, become misaligned with the light path. Such misalignment significantly reduces image quality; thus, the position and orientation of primary mirror (POPM) control systems must maintain the optical axis in an ideal position. Therefore, in this paper, we propose a novel high-accuracy electrohydraulic control system for the position and orientation of the primary mirror (POPM) of a large telescope. To this end, a POPM control system with five electrohydraulic partitions is adopted, and a mathematical model of the POPM is derived. In addition, a mathematical model of each partition of the electrohydraulic system is derived for the telescope controller design. A linear active disturbance rejection controller (LADRC) and a sliding mode controller (SMC) are adopted in each electro-hydraulic partition to ensure positioning accuracy. Experiments are carried out on 4 and 1.2 m large telescopes. The corresponding results show that by both keeping constant and varying the elevation of the large telescopes, the position error of the primary mirror can be limited to less than 1 μm , and the orientation of the primary mirror can be maintained with an error of less than 0.05 arcsec, even in the presence of external disturbances. This control accuracy can guarantee both the inalterability of the optical axis of the primary mirror and the possibility to adjust the light according to the requirement in order to obtain high-resolution images.

Keywords Large telescope · Primary mirror support · Electrohydraulic control system

1 Introduction

In recent years, the size of the primary mirrors of ground-based optoelectronic telescopes has been consistently increased in order to track astronomical objects in deep space with higher imaging resolutions. Due to variations in gravity, temperature, and external disturbances, the position and the orientation of the primary mirror (POPM) changes more as the diameter of a telescope increases. The light is reflected by the primary mirror and then is converged to the secondary mirror to form the optical axis, but due to the POPM changes, the primary and the secondary mirrors may become misaligned when the telescope moves to a different position [1–4]. This can cause blurring, coma, and astigmatism, which can seriously degrade the telescope's image

quality and even cause images to shift out of the telescope's field of view.

The relative position between the primary and the secondary mirrors is influenced by several factors: the gravity deformations of the secondary mirror, elastic deformations of the primary mirror support system, and deformation of the POPM relative to the primary mirror cell [5–10]. The primary mirror is always installed in the primary mirror cell and is supported by the POPM control system in the primary mirror cell, which is fixed on the telescope. The position between the primary mirror cell and the telescope can be considered as invariable. However, the POPM relative to the primary mirror cell may change due to variations in gravity, temperature, and external disturbances when working under different conditions. The POPM must be kept constant in order to maintain an ideal optical axis, and the position and orientation (PO) of the secondary mirror can be adjusted to point to the ideal optical axis [11, 12]. If the POPM cannot be stably controlled, the secondary mirror cannot be adjusted by transformations. This paper's focus is on

✉ Yu-Xia Li
lyx26691023@163.com

¹ Changchun Institute of Optics, Fine Mechanics and Physics, Chinese Academy of Sciences, Changchun, China

the solution to adjusting the POPM relative to the primary mirror cell in order to obtain an ideal optical axis.

Thus far, a hydraulic or pneumatic POPM control system and a Stewart platform to control the secondary mirror have usually been adopted [13, 14]. The hydraulic system is more stable and more rigid, and has an outstanding anti-interference ability due to its higher number of supporting points [7–12]. The 8 m Very Large Telescope in European Southern Observatory [1], the 8 m Gemini telescope, and the 4 m Advanced Electro-Optical System telescope in the USA [7, 10, 11] employ hydraulic control systems whereas the Multiple Mirror Telescope employs a Stewart platform [13]. However, the existing literature does not provide enough details on the POPM control system or on experimental results.

To attain the required imaging accuracy, for our study, we chose an electrohydraulic system to control the POPM of 4 and 1.2 m large telescopes. Based on a study of possible systematic detail-resolving methods that could be adopted for the POPM and in order to obtain a high-precision control, we could flexibly adjust three axial and two lateral hydraulic partitions are by using sliding mode controllers (SMC) and linear active disturbance rejection controllers (LADRC). The experimental results indicated that a high image quality could be achieved with this method.

2 Operating principle of POPM control

The POPM control system helps to control the POPM relative to the primary mirror cell. The operating principle of the POPM control is shown in Fig. 1. The large telescope contains both the primary and the secondary mirrors. The primary mirror is installed in the primary mirror cell and is always maintained in the same position. The optical axis of the primary mirror shifts as the POPM changes, and variations in elevation angle, temperature, and wind strongly influence the POPM. When the ideal optical axis that connects the primary mirror to the secondary mirror shifts, the POPM needs to be adjusted. Five partitions (three axial and two lateral) are used to support the primary mirror. Three axial and two lateral partitions, respectively, support the axial and the lateral weights separately. These five displacement sensors are dispersedly installed on the primary mirror to monitor the POPM. The regulation components of each partition consist of displacement sensors, servo motor drivers, and permanent-magnet synchronous motors (PMSMs) to drive the electric and hydraulic multi-supporting cylinders located under the primary mirror.

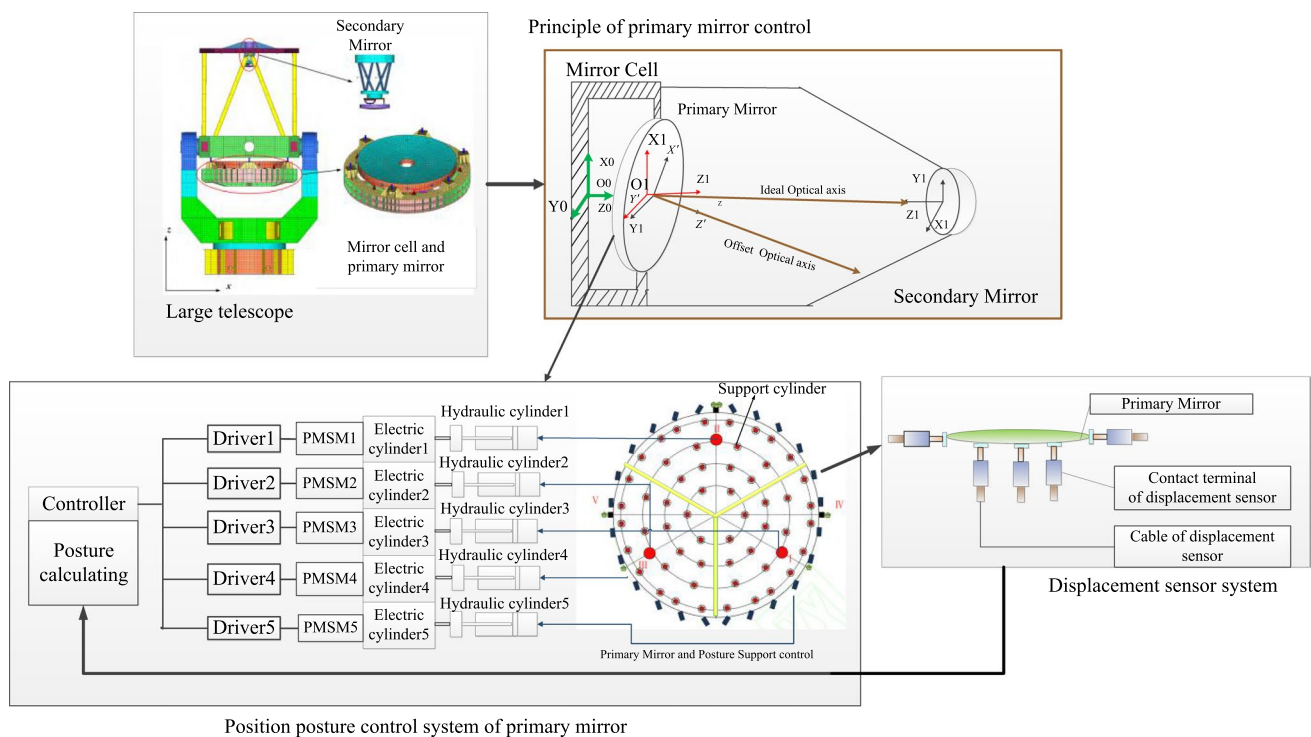


Fig. 1 Operating principle of the POPM control

2.1 POPM displacement sensor system

The primary mirror has six degrees of freedom in space; however, one displacement sensor installed under the primary mirror can measure a shift only in one direction. Therefore, in order to cover all six degrees of freedom, we propose to use five displacement sensors located in different positions on the primary mirror. The ideal POPM can be calculated on the basis of the ideal optical axis and recorded as the initial value. The actual POPM can be obtained using the displacement sensors when the telescope changes its position. The displacement of each partition can be obtained by comparing the ideal POPM with the actual POPM, which can be achieved with a new camera detector. In addition, an algorithm that reproduces the proposed solution, which can be implemented based on a position adjusting unit, is used to adjust the POPM.

To calculate the displacement of each partition, we built a mathematical model of the primary support system. Figure 2 shows a simplified model of the primary mirror support system. The primary mirror can be considered as a moving plane supported by three parallel and homologous electrohydraulic cylindrical actuators.

Three virtual connection points act on the primary mirror and its cell. The primary mirror cell is defined in a static O - XYZ coordinate system, and the primary mirror is defined in a dynamic O_1 - $X_1Y_1Z_1$ coordinate system. All the cylindrical actuators used to support the primary mirror move in the O - XYZ coordinate system. The three virtual supporting points of the primary mirror can be transformed into three virtual supporting points in the static coordinate system by using a matrix φ_α . Let O_1 be the center of the O_1 - $X_1Y_1Z_1$ coordinate system; $A_1 = [R_1, 0, 0, 1]^T$, $B_1 = \left[\frac{-R_1}{2}, \frac{\sqrt{3}R_1}{2}, 0, 1 \right]^T$, and $C_1 = \left[\frac{-R_1}{2}, \frac{-\sqrt{3}R_1}{2}, 0, 1 \right]^T$

, where $A_1, B_1,$ and C_1 are the three virtual supporting points of the primary mirror; $A = [R, 0, 0, 1]^T$, $B = \left[-\frac{R}{2}, \frac{\sqrt{3}R}{2}, 0, 1 \right]^T$, and $C = \left[-\frac{R}{2}, -\frac{\sqrt{3}R}{2}, 0, 1 \right]^T$, where $A, B,$ and C are the corresponding virtual supporting points in the static coordinate system O - XYZ of the cell; R_1 the distance between the virtual supporting point and the center of the primary mirror; and R the distance between the virtual supporting point and the center of the cell. Any point on the static coordinate system can be converted to its corresponding point in the dynamic coordinate system. Let M_{xp} , M_{yp} , and M_{zp} be the translation transformations from the dynamic coordinate system to the static coordinate system in the x -direction, y -direction, and z -direction, respectively. Finally, let ϕ_α be the rotation angle around the x -axis, ϕ_β the rotation angle around the y -axis, and ψ_γ the rotation angle around the z -axis. The conversion matrix that relates the virtual supporting points in the static system to the corresponding supporting points in the dynamic system is

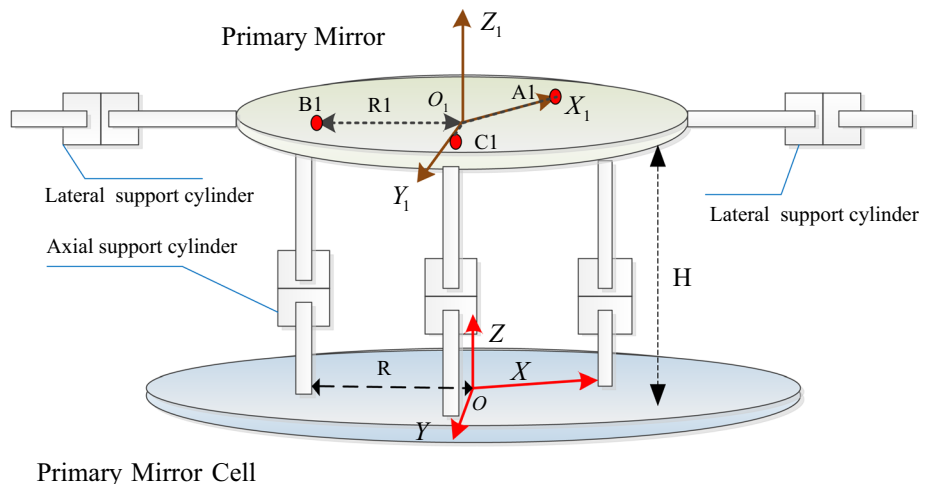
$${}^U T_V = R(\phi_\alpha, \phi_\beta, \psi_\gamma, M) = Rot(Z, \phi_\alpha)Rot(Y, \phi_\beta)Rot(X, \psi_\gamma) = \begin{bmatrix} C\phi_\alpha C\phi_\beta & C\phi_\alpha S\phi_\beta S\psi_\gamma - S\phi_\alpha C\psi_\gamma & C\phi_\alpha S\phi_\beta C\psi_\gamma + S\phi_\alpha C\psi_\gamma & M_{xp} \\ S\phi_\alpha C\phi_\beta & S\phi_\alpha S\phi_\beta S\psi_\gamma + C\phi_\alpha C\psi_\gamma & S\phi_\alpha S\phi_\beta C\psi_\gamma - C\phi_\alpha C\psi_\gamma & M_{yp} \\ -S\phi_\beta & C\phi_\alpha S\psi_\gamma & C\phi_\alpha C\psi_\gamma & M_{zp} \\ 0 & 0 & 0 & 1 \end{bmatrix} \tag{1}$$

Let C be the cosine, S the sine, ${}^V p$ the transformation matrix that expresses point p on the primary mirror in the O_1 - $X_1Y_1Z_1$ system, and ${}^U p$ the transformation matrix that expresses point p in the O - XYZ system. Therefore, the position of point p relative to the primary mirror cell's position can be defined as follows:

$${}^U p = {}^U T_V \times {}^V p \tag{2}$$

In addition, the position of the three supporting points A_1, B_1, C_1 on the primary mirror relative to the position of the primary cell can be derived as

Fig. 2 Simplified model of the primary mirror support system



$${}^0I = [{}^0A_1; {}^0B_1; {}^0C_1] = [A_1; B_1; C_1] \times {}^U T_V, \quad (3)$$

where 0A_1 , 0B_1 , and 0C_1 are the corresponding points of A_1 , B_1 , and C_1 in the static coordinate system. The transform matrix can be simplified as

$${}^U T_V = \begin{bmatrix} n_x & o_x & a_x & X_p \\ n_y & o_y & a_y & Y_p \\ n_z & o_z & a_z & Z_p \\ 0 & 0 & 0 & 1 \end{bmatrix} \quad (4)$$

and the displacement l_i of each partition can be expressed as follows:

$$l_i = \|{}^0I_i - J_i\|_2, \quad i = 1, 2, 3, \quad (5)$$

where $J = [A; B; C]$. Therefore, the decoupled movement of each virtual supporting point can be derived from Eqs. (1)–(5) as follows:

$$l_i = \sqrt{l_n^2 + l_o^2 + l_a^2} \quad (6)$$

The solutions are

$$\begin{aligned} l_1^2 &= (R_1 n_x + X_p - R)^2 + (R_1 n_y + Y_p)^2 + (R_1 n_z + Z_p)^2, \\ l_2^2 &= \left(\frac{-R_1 n_x}{2} + \frac{\sqrt{3} R_1 o_x}{2} + X_p + \frac{R}{2} \right)^2 + \left(\frac{-R_1 n_y}{2} + \frac{\sqrt{3} R_1 o_y}{2} + Y_p - \frac{\sqrt{3} R}{2} \right)^2 + \left(\frac{-R_1 n_z}{2} + \frac{\sqrt{3} R_1 o_z}{2} + Z_p \right)^2, \\ l_3^2 &= \left(\frac{-R_1 n_x}{2} - \frac{\sqrt{3} R_1 o_x}{2} + X_p + \frac{R}{2} \right)^2 + \left(\frac{-R_1 n_y}{2} - \frac{\sqrt{3} R_1 o_y}{2} + Y_p + \frac{\sqrt{3} R}{2} \right)^2 + \left(\frac{-R_1 n_z}{2} - \frac{\sqrt{3} R_1 o_z}{2} + Z_p \right)^2. \end{aligned} \quad (7)$$

Equation (7) allowed the POPM to be adjusted by taking into account the values of the displacement sensors. The POPM can be calculated and expressed as

$$\begin{cases} Z = \frac{l_1 + l_2 + l_3}{3} - \frac{l_{10} + l_{20} + l_{30}}{3}, \\ Rx = \arctan \frac{2l_1 - l_2 - l_3}{\sqrt{3}R} - \arctan \frac{2l_{10} - l_{20} - l_{30}}{\sqrt{3}R}, \\ Ry = \arctan \frac{l_2 - l_3}{\sqrt{3}R} - \arctan \frac{l_{20} - l_{30}}{\sqrt{3}R}, \end{cases} \quad (8)$$

where l_{10} , l_{20} , and l_{30} are the initial positions of five displacement sensors. Any variation in Z will generate image defocus, and any rotation offset of Rx and Ry will cause coma and spherical aberration, which cause optical dispersion and greatly reduce the image quality.

Suppose the focal ratio of the large telescope is f and the diameter of telescope primary mirror is D , then, the position and the posture shifts of primary mirror mapping

to the secondary mirror can be calculated using the following equations:

$$\begin{cases} Z_{\text{sec ond}} = Z, \\ Rx_{\text{sec ond}} = f * D * \tan(Rx), \\ Ry_{\text{sec ond}} = f * D * \tan(Ry). \end{cases} \quad (9)$$

With Eqs. (8) and (9), this shift of the position and the posture acting on the second mirror can be calculated, the sensitivity of the primary and the secondary mirrors under an operation environment can be described, and the shift of the position and the posture acting on the second mirror will cause a diffuse spot of the optics system, which is related to D , f , Rx and Ry . Where the size of diffuse spot can describe the imaging quality.

2.2 Model and control method of each partition

As mentioned before, the primary mirror control system has three axial and two lateral partitions, and for each partition, a hydraulic drive unit that moves the hydraulic cylinders installed under the primary mirror. The three axial and the two lateral partitions have 54 and 24 supporting cylinders, respectively. The upper chambers that host the axial hydraulic cylinders are connected to each other

and to an axial accumulator, which is used to stabilize the oil pressure. The upper chambers that host the lateral hydraulic cylinders are also connected to each other and to a lateral accumulator. On the other hand, the bottom chambers that host the three axial and the two lateral partitions are controlled separately using oil volume adjustment units, that are made of electric and hydraulic cylindrical units (EU). The electric cylinders have PMSMs and roller screws that drive the oil-filled hydraulic cylinders. When the electric cylinders move, the hydraulic cylinders inject or extract oil from the supporting hydraulic cylinders; then, the oil pressure of the bottom chambers will increase or decrease, causing a difference in oil pressure between the upper and the bottom chambers. Therefore, the POPM can be adjusted by moving the supporting hydraulic cylinders; this process is described in Figs. 3 and 4:

The corresponding model can be derived, based on the oil flow, from the following equations:

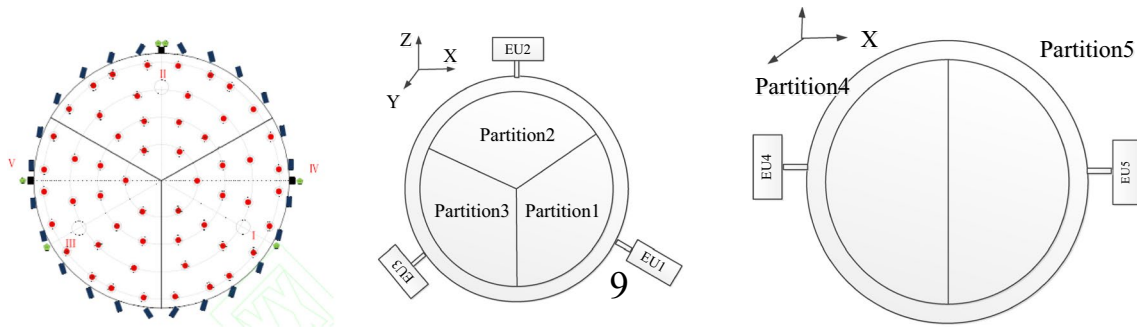


Fig. 3 General structure of the five partitions

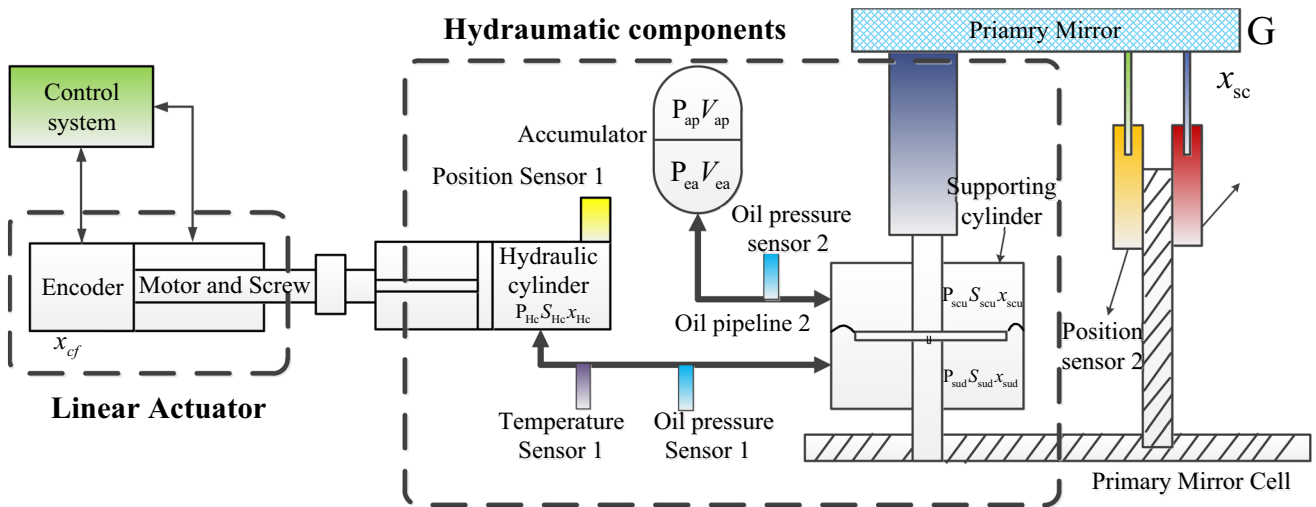


Fig. 4 Architecture of a single hydraulic control partition

$$\begin{cases} -A_{Hc} \frac{dX_{Hc}}{dt} + \frac{V_{Hc0} - A_{Hc} X_{Hc}}{E_h} \frac{dP_{Hc}}{dt} = Q_{Hc}, \\ -A_{sc} \frac{dX_{sc}}{dt} + \frac{V_{scd0} - A_{sc} X_{sc}}{E_h} \frac{dP_{scd}}{dt} = Q_{scd}, \\ -A_{sc} \frac{dX_{sc}}{dt} + \frac{V_{scu0} - A_{sc} X_{sc}}{E_h} \frac{dP_{scu}}{dt} = -Q_{scu}, \\ \frac{dV_{ea}}{dt} + \frac{V_{ea}}{E_h} \frac{dP_{pea}}{dt} = Q_{pea}, \end{cases} \quad (10)$$

where A_{Hc} and A_{sc} are the effective areas of the servo hydraulic cylinders and of the supporting hydraulic cylinders, respectively; X_{Hc} and X_{sc} are the displacements of the hydraulic cylinders and of the supporting hydraulic cylinders when the POPM changes; V_{Hc0} , V_{scd0} , V_{scu0} , and V_{ea} are the initial oil volume of the servo hydraulic cylinders, the upper chambers of the supporting cylinders, the bottom chambers of the supporting cylinders, and the accumulator, respectively; P_{Hc} , P_{scd} , P_{scu} , and P_{pea} are the oil pressure of the servo hydraulic cylinders, the upper chambers of the supporting hydraulic cylinders, the bottom chambers of the supporting hydraulic cylinders, and the accumulator, respectively; and

Q_{Hc} , Q_{scd} , Q_{scu} , Q_{pea} are the oil flows into the servo hydraulic cylinders, the upper chambers of the supporting cylinders, the bottom chambers of the supporting cylinders, and the accumulator, respectively. Based on the principle of communicating vessels, we have.

$$P_{Hc} = P_{scd}, P_{scu} = P_{pea}, Q_{Hc} = Q_{scd}, Q_{scu} = Q_{pea}. \quad (11)$$

Ignoring the negligible terms in the formula, the equation can be simplified as follows:

$$\begin{aligned} A_{sc} \frac{dX_{sc}}{dt} - A_{Hc} \frac{dX_{Hc}}{dt} &= \frac{A_{sc} X_{sc} - A_{Hc} X_{Hc} - (V_{scd0} + V_{scu0})}{E_h} \frac{dP_{Hc}}{dt} \\ &\approx -\frac{(V_{scd0} + V_{scu0})}{E_h} \frac{dP_{Hc}}{dt} = \frac{-V_{sc}}{E_h} \frac{dP_{Hc}}{dt}. \end{aligned} \quad (12)$$

In addition, based on the pneumatic-state equation of an airbag-type accumulator [15, 16] the pressure of the accumulator can be considered constant:

$$P_{ap} V_{ap} = \text{CONST}, \tag{13}$$

where P_{ap} is the air pressure and V_{ap} is the air volume.

It follows that

$$\frac{dP_{ap}}{dt} V_{ap0} + \frac{dV_{ap}}{dt} P_{ap0} = 0 \tag{14}$$

When Eqs. (13) and (14) are taken into account, Eq. (12) can be written as

$$A_{sc} \dot{X}_{SC} = \frac{V_{ap0}}{P_{ap0}} \frac{dP_{scd}}{dt} + \frac{V_{scu} + V_{scd} - A_{sc} X_{sc}}{E_h} \frac{dP_{scd}}{dt}. \tag{15}$$

Considering that the working oil pressure of the system is between 5 and 7 bars,

$$P_{ap0} \ll E_h \tag{16}$$

Thus, we have

$$\frac{V_{ap0}}{P_{ap0}} \gg \frac{V_{scu} + V_{scd} - A_{sc} X_{sc}}{E_h} \tag{17}$$

Equation (15) can be written as

$$A_{sc} \dot{X}_{SC} \approx \frac{V_{ap0}}{P_{ap0}} \frac{dP_{scd}}{dt}. \tag{18}$$

When the influence of the constant high rigidity of the hydraulic cylinder is neglected, the dynamic balance motion equation of supporting cylinders can be expressed as

$$M_{mi} \cos(EL) \ddot{X}_{sc} + B_{sc} \dot{X}_{SC} = A_{sc}(P_{Hc} - P_{scd}) - G - F_L, \tag{19}$$

where $M_{mi} \cos \delta$ is the weight of the primary mirror on each partition, EL is the elevation angle of the large telescope, \ddot{X}_{sc} is the acceleration, B_{sc} is the damping parameter, X_{sc} is the velocity of supporting cylinders, G is the gravity that acts on the supporting cylinders, and F_L is the external force applied on the supporting cylinders, which includes friction and other external interferences.

The displacements of the supporting cylinders of each partition, X_{sci} , can be measured through a linear variable differential transformer (LVDT), and X_{sci} can be expressed as l_i in Eq. (6). On the basis of Eqs. (8), (12)–(16) and with external disturbances neglected, the transfer function from the hydraulic cylinders' displacements to the supporting cylinders' displacements can be expressed as,

$$\begin{aligned} \frac{X_{sc}(s)}{X_{Hc}(s)} &= \frac{A_{Hc}/A_{sc}}{V_{sc} M_{mi} \cos \delta s^2 / A_{sc}^2 E_h + V_{sc} B_s / A_{sc}^2 E_h + 1 + V_{sc} P_{ap0} / V_{apo} E_h} \\ &= \frac{A_{Hc}/A_{sc}}{V_{sc} M_{mi} \cos \delta s^2 / A_{sc}^2 E_h + V_{sc} B_s / A_{sc}^2 E_h + 1} \end{aligned} \tag{20}$$

The transfer function is a second-order relation, where the elevation angle of the large telescope is a second-order term.

The electrical and torque balance equation of the electric cylinders [15], consisting of PMSMs and ball screws, can be expressed as,

$$\left\{ \begin{aligned} u_q &= R_a i_q + L_q \frac{di_q}{dt} + \omega_r (L_d i_d + \psi_f), \\ u_d &= R_a i_d + L_q \frac{di_d}{dt} - \omega_r L_d i_d, \\ T_e &= 1.5 n_p [\psi_f i_q + L_d - L_q i_d i_q], \\ T_e &= T_d + B\omega + J \frac{d\omega}{dt}, \\ \omega &= \frac{d\theta}{dt}, \\ X_{Hc} &= X_a = \frac{\theta L_s}{2\pi}, \\ T_d &= \frac{P_{Hc} A_{Hc}}{2\pi \eta}, \end{aligned} \right. \tag{21}$$

where u_q and i_q are the voltage and the current of the motor quadrature axis, respectively; u_d and i_d are the voltage and the current of the motor direct axis, respectively; R_a is the electrical resistance; ω_r is the electrical angle; ψ_f is the flux linkage of the permanent magnet; T_e is the output torque; T_d is the load torque; B is the damping coefficient; J is the moment of inertia of the motor; n_p is the number of motor poles; θ is the rotation angle; ω is the rotation velocity; and η is the transmission efficiency. The transfer function between the linear displacement of the electric cylinders and the output current of the motor can be expressed as

$$X_{Hc}(s) = \frac{\theta L_s}{2\pi} \frac{1.5 n_p \psi_f}{s(Js + \kappa) \left(\frac{L_q}{R_a} s + 1 \right)} I_q(s). \tag{22}$$

Equation (21) shows that, also in this case, the transfer function is a second-order relation that depends on electrical and mechanical parameters. The position and the current speed of the closed-loop control system for the PMSM were also designed. A PI controller using the pole-zero elimination method is applied in the current loop. To neglect the effect of the external friction, the force used to correct the mirror shape, temperature variations, and external disturbances, we designed the LADRC in the velocity loop and the SMC in the position loop.

When the torque fluctuation of the mutual inductance ($\omega_r(L_d i_d + \psi_f)$) is neglected, the open-loop transfer function

of the current loop with a PI controller can be represented as follows:

$$G_o(s) = K_p \left(1 + \frac{1}{T_i s} \right) \left(\frac{1}{L_d s + R_s} \right) \tag{23}$$

when T_i is expressed as $\frac{L_d}{R_s}$, the closed-loop transfer function of the current can be expressed as

$$G_o(s) = \frac{G_c(s)}{1 + G_c(s)} = \frac{1}{\frac{L_d}{K_p} s + 1} \tag{24}$$

The time constant of the current loop can be changed from $\frac{L_d}{R_s}$ to $\frac{L_d}{K_{pi}}$, where $\frac{L_d}{K_{pi}}$ is the cut-off frequency of the current loop. The phase delay of this first-order inertial system can be reduced by adjusting K_{pi} , so that the velocity loop can be easily designed. The current loop can be considered to be equal to 1 when the designed bandwidth is 5 times higher than velocity loop's bandwidth. To compensate for the non-linearity of the electric cylinder system and the effect of external disturbances, we designed the velocity loop adopted in LADRC with a linear extended state observer (ESO). This control system is designed to estimate combined external disturbances by using input and output information and then, in order to limit internal and external interferences, to add the corresponding feedback compensation to the output of the speed controller. This control algorithm depends neither on the system model nor on the linearity of the system, and efficiently reduces internal and external interferences.

The differential equation of the velocity loop can be written as

$$\dot{y} = f(y, \ddot{y}, t) + bu, \tag{25}$$

where y represents the measured speed of the system, u the current, b the gain, and $f(y, \ddot{y}, t)$ the all unmolded part except for the control output. With y and u , the ESO can be defined as follows:

$$\begin{cases} \dot{z}_1 = z_2 + bu - \beta_1 g_1(e_1), \\ \dot{z}_2 = -\beta_2 g_2(e_1), \end{cases} \tag{26}$$

where $e_1 = z_1 - y, \beta_1$, and β_2 are parameters to be defined, $g_1(e_1)$ and $g_2(e_1)$ are the function's estimated errors. Equation (25) yields $g_i(e)e > 0, e \neq 0$, and with a proper definition of β_1 and β_2 , $z_1 \rightarrow y$ and $z_2 \rightarrow f$. For simplicity of implementation, β_1 and β_2 can be expressed as

$$\begin{cases} \beta_1 = -2w_o, \\ \beta_2 = -w_o^2, \end{cases} \tag{27}$$

where w_o represents the bandwidth of ESO, and z_2 is the f estimator, which can be introduced in the controller design to compensate for noise. The controller can be defined as follows:

$$u = \frac{K_{pv}(y^* - y) - z_2}{b}, \tag{28}$$

Therefore, the closed-loop system can be expressed as

$$\dot{y} = K_{pv}(y^* - y), \tag{29}$$

and the approximate transfer function of the closed-loop is

$$G_{close}(s) \approx \frac{K_{pv}}{s + K_{pv}} \tag{30}$$

The parameter K_{pv} is close to the bandwidth of the closed loop system. The controller can be well designed by adjusting the K_{pv} parameter. Once the speed loop and the current loop have been designed, the system response can be considered to be equal to 1. On the other hand, the position loop can be designed by considering it as a second-order system. In order to eliminate the position error related to the different elevations and working conditions of the telescope, and to ensure that the system can detect the target quickly and stably, we adopted a feedforward controller (EEFC) in the SMC. The hydraulic system position loop can be expressed as

$$G_{op} = \frac{K}{As^2 + Bs + c} \frac{K_{pv}}{s + K_{pv}}, \tag{31}$$

where $K = L_s A_{Hc} / 2\pi A_{sc}$, $A = V_{sc} M_{mi} \cos \delta / A_{sc}^2 E_h$, $B = V_{sc} B / A_{sc}^2 E_h$, and $c = 1$. Because the response of the velocity loop can be considered equal to 1, the equation of state of the position loop can be written as follows:

$$\ddot{x}_{sc} = A\dot{x}_{sc} + k\dot{x}_{Hc} + cx_{Hc} \tag{32}$$

Because the rigidity of the hydrodynamic system is constant, we can consider $x(1) = x_{Hc}$, and $x(2) = \dot{x}_{Hc}$, and we can rewrite Eq. (32) as

$$\dot{x} = \mathbf{A}_1 \mathbf{x} + \mathbf{B}_1 \mathbf{u} \tag{33}$$

where $\mathbf{x} = \begin{bmatrix} x(1) \\ x(2) \end{bmatrix}$, $\mathbf{A}_1 = \begin{bmatrix} 0 & 1 \\ 0 & -\frac{B}{A} \end{bmatrix}$, and $\mathbf{B}_1 = \begin{bmatrix} 0 \\ \frac{K}{A} \end{bmatrix}$.

disturbance, we carried out the experiments by using a force that shapes the primary mirror under different control methods.

The POPM of the 4 m large telescope is shown in Fig. 7. Figure 7a shows the inclination in the x -direction and in the y -direction (R_x and R_y , respectively) and the shift in the z -direction (Z). R_x ranges from -0.5 to 1 arcsec, R_y ranges from -3.5 to 0.5 arcsec, and Z is about $10 \mu\text{m}$. Figure 7b shows a two-dimensional plot of R_y as a function of R_x , which further demonstrates that the displacements of the optical axis are not focused on a point but on a line. Figure 8a shows the results obtained with the 4 m large telescope whose elevation axis moves at a speed of $1^\circ/\text{s}$ without control. The corresponding LVDT displacements are shown in Fig. 8b. The position of the elevation axis changes from 85° to 5° in 90 s. Figure 8b also shows that the axial and the lateral LVDT errors are up to 120 and $700 \mu\text{m}$, respectively.

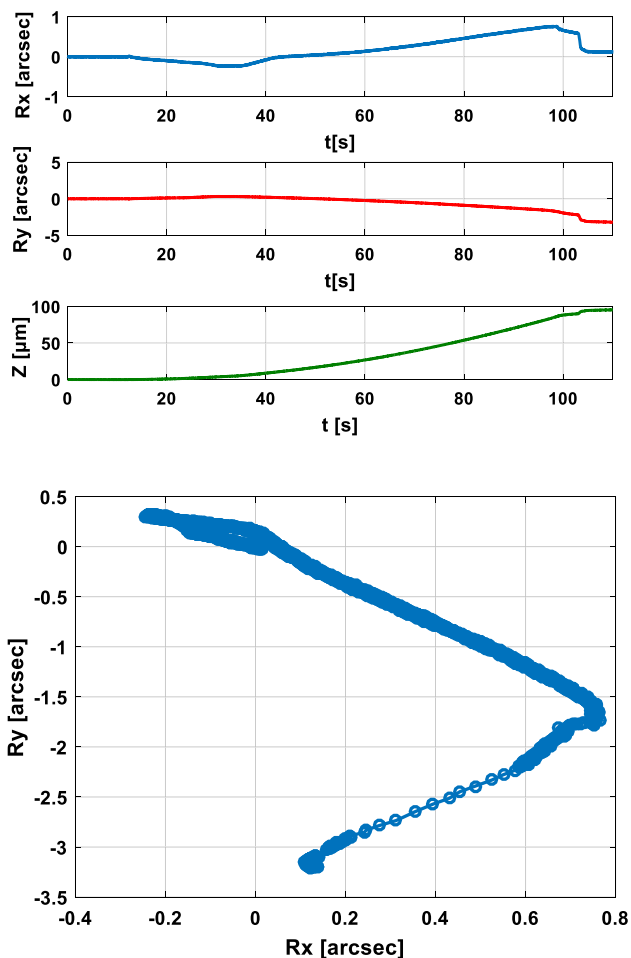


Fig. 7 POPM characteristics of the 4 m large telescope whose elevation axis moves at a speed of $1^\circ/\text{s}$ without control: **a** Inclinations in the x -direction and the y -direction (R_x and R_y , respectively) and the shift in the z -direction (Z) and **b** two dimensional tilt migration of the POPM

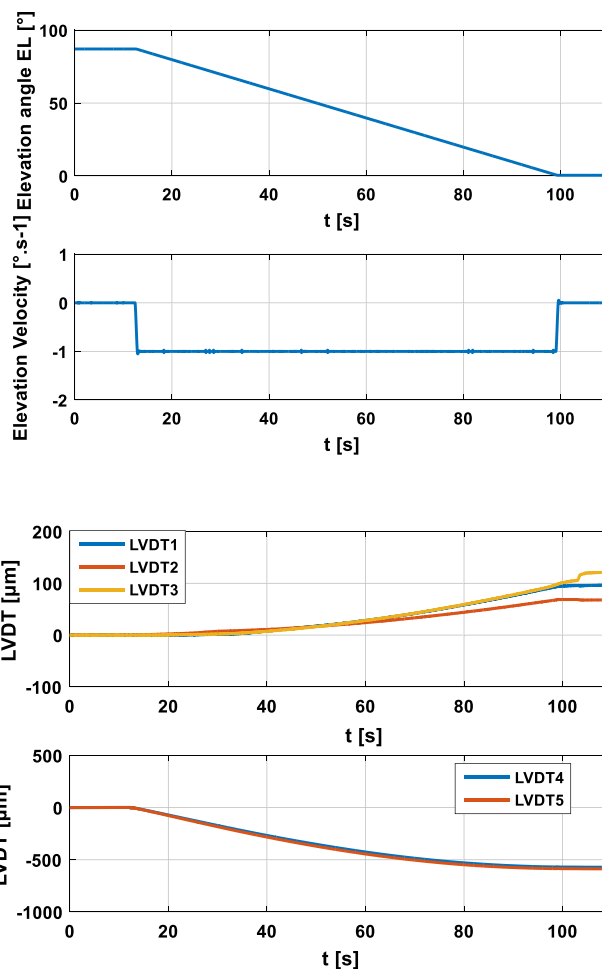


Fig. 8 LVDT displacements needed to adjust at a $1^\circ/\text{s}$ elevation speed without control. **a** Elevation speed and angle of the POPM of the 4 m large telescope, whose elevation axis moves at a speed of $1^\circ/\text{s}$ without control and **b** LVDT displacements needed to adjust of the POPM

These errors correspond to the displacements that the five partitions must undergo to obtain an ideal optical axis.

The same calculations were performed using the 4 m large telescope whose elevation axis moves at a controlled speed of $1^\circ/\text{s}$ upon when the ADRC and the SMC controllers are used. The results are shown in Figs. 9 and 10. Figure 9a shows that the R_x and the R_y inclinations stay within 0.01 arcsec and that the Z shift of the PM can be limited to $1 \mu\text{m}$ owing to the controller. Figure 9b shows the two-dimensional variation of the POPM's inclination. When the ADRC and the SMC controllers are used, the displacements of the optical axis can be focused on one point, which is only about 0.01 arcsec. Figure 10 proves that when the elevation axis moves at $1^\circ/\text{s}$ from 85° to 15° , the five LVDT displacement errors can all be limited to $1 \mu\text{m}$ by using a controller.

For further verification of the POPM control system, another set of experiments was carried out using the 1.2 m large telescope, and a vibrational speed was applied to

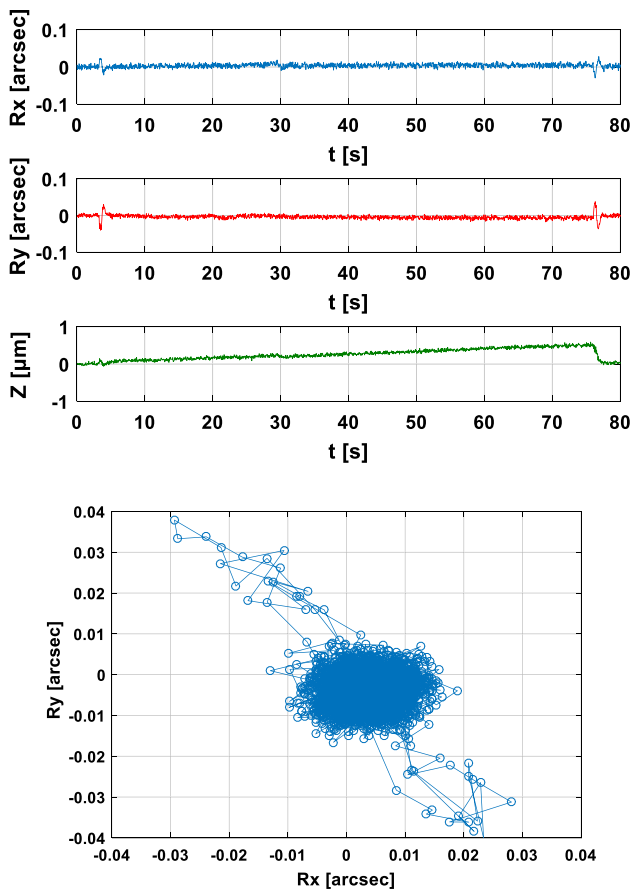


Fig. 9 POPM characteristics of the 4 m large telescope whose elevation axis moves at a controlled speed of $1^\circ/\text{s}$ when the ADRC and SMC controllers are used. **a** Inclinations in the x-direction and the y-direction (R_x and R_y , respectively) and the shift in the z-direction (Z) and **b** twodimensional plot of R_y as a function of R_x

its elevation axis. Figure 11a shows that R_x and R_y are about $0 \sim 1$ and 0.2 arcsec, respectively, and that Z is about $-10 \mu\text{m}$. The inclination trend is more intuitive in Fig. 11b, where a two-dimensional plot shows that the axis undergoes irregular displacements from the ideal point. Figure 12a shows that the position moves from 0° to 60° and then back to 0° at a vibrational speed that reaches a maximum of about $10^\circ/\text{s}$ and whose trend is similar to that of a sinusoid. Figure 12b shows that the axial and the lateral partitions must be displaced by a maximum of 10 and $100 \mu\text{m}$, respectively. These displacements are smaller than those obtained with the hydraulic system of the 4 m large telescope due to the smaller elevation and the lower weight of the 1.2 m large telescope.

The results obtained by using the control system are shown in Fig. 13. In this case, R_x and R_y are less than 0.01 arcsec, and Z is less than $0.4 \mu\text{m}$. The two-dimensional plot in Fig. 14b shows that the actual axis can focus on a point of 0.01 arcsec, although very few fluctuations appear

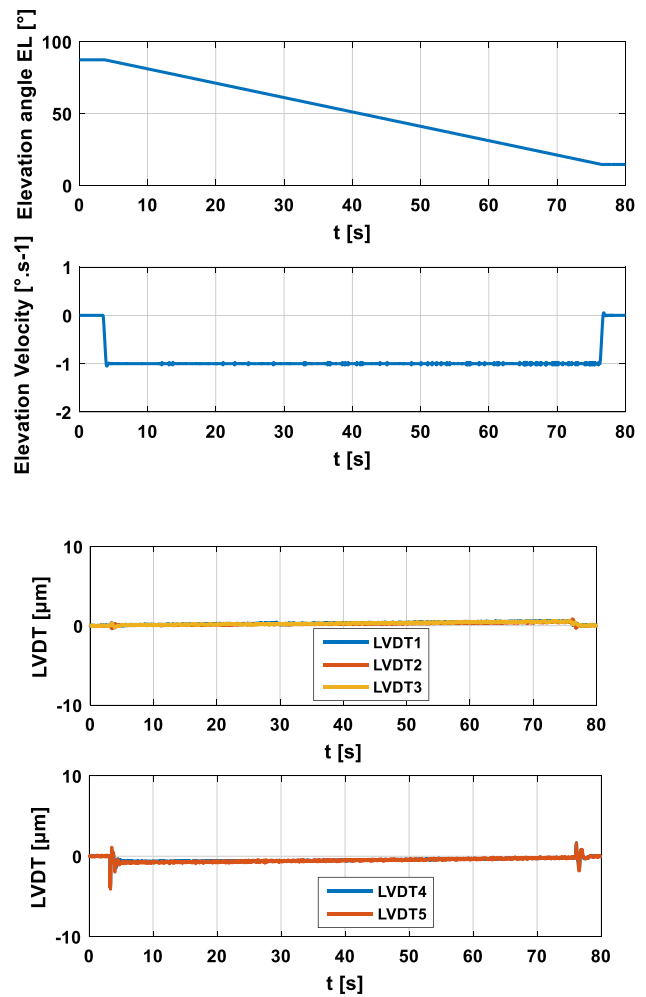


Fig. 10 The LVDT displacements needed to adjust at a $1^\circ/\text{s}$ elevation speed with control. **a** Elevation speed and angle of the POPM of the 4 m large telescope, whose elevation axis moves at a controlled speed of $1^\circ/\text{s}$ when ADRC and SMC controllers are used and **b** LVDT displacements needed to adjust

in the transition process due to the high speed adopted for this case.

Figure 14 shows the LVDT errors of the five partitions when the elevation changes at different speeds, which is the most common case in practical applications. The errors are all within $1 \mu\text{m}$, which is comparable to the error corresponding to the optical axis position after compensation.

In order to evaluate the performance of the proposed SMC and ADRC controllers, we take the external noise into consideration and carried out, further experiments were carried out on the primary mirror of the 1.2 m large telescope. A force of 280 N was applied on the mirror while it was held in a stationary position. Figure 15 shows that under three different control conditions, the optical axis moves by a maximum of 1 arcsec in an irregular manner. The displacements can be reduced using a PI controller with well-defined

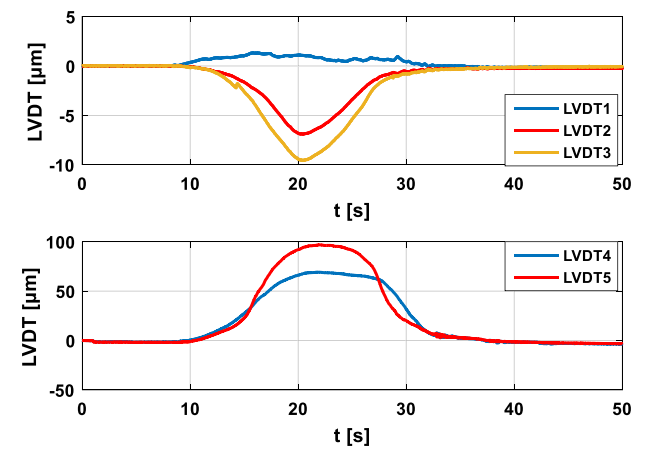
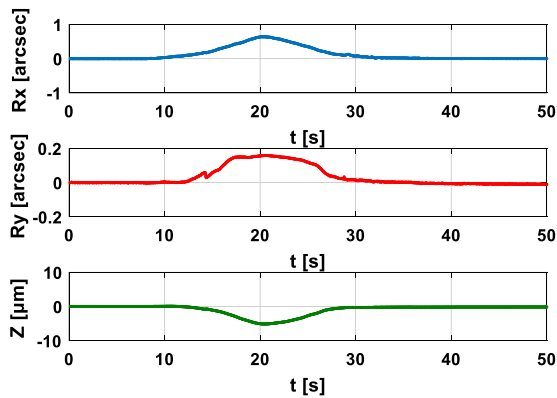
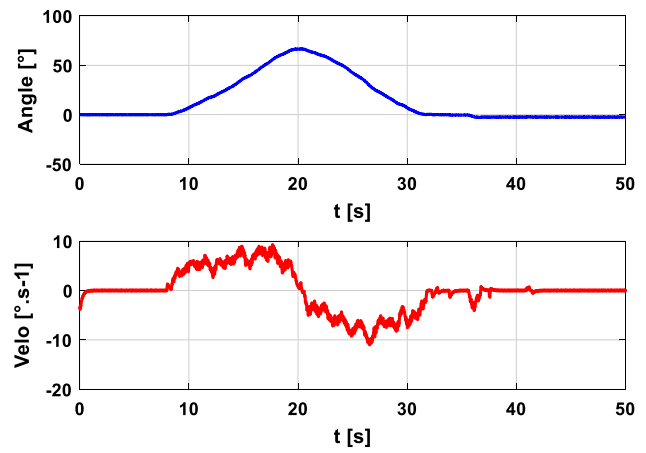
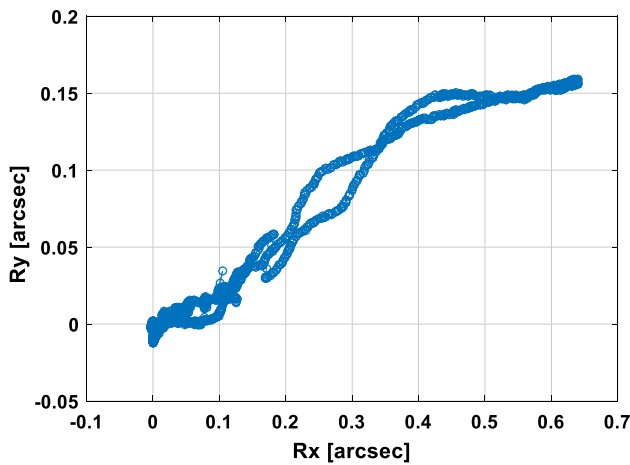


Fig. 11 POPM characteristics of the 1.2 m large telescope whose elevation axis moves at a vibrational speed without control: **a** Inclinations in the x -direction and the y -direction (R_x and R_y , respectively) and the shift in the z -direction (Z); **b** two-dimensional plot of R_y as a function of R_x

Fig. 12 LVDT displacement needed to adjust at a vibrational elevation speed without control: **a** Elevation speed and angle of the POPM of the 1.2 m large telescope, whose elevation axis moves at a vibrational speed without control and **b** LVDT displacement needed to adjust

parameters. In this case, the shift is circular because of the transient response process of the hydraulic system. Finally, when the SMC and ADRC controllers are used, the displacement can be reduced to a point with a radius smaller than 0.03 arcsec.

4 Conclusions

In this study, a hydraulic control system and a mathematical model are defined to regulate the displacements of the POPM. Furthermore, in order to correctly adjust the POPM, we analyzed the LVDT displacements of five partitions. The hydraulic support system and the electronic control system of each partition are also modeled. A high-precision control

of the position of the primary mirror is achieved using an ADRC and SMC. The results show that for 4 and 1.2 m large telescopes, the inclinations in the x -direction and the y -direction can be limited to 0.04–3.5 and 0.01–0.15 arcsec, respectively, to ensure that the axis displacement stays on one point when the elevation changes. The elevation of the 4 and 1.2 m large telescopes was changed at a constant speed of 1°/s and at a variable speed, respectively. Furthermore, when a force of 280 N is applied on the primary mirror, the inclinations of the POPM in the x -direction and the y -direction can be limited to 0.03–0.9 arcsec by using the ADRC and the SMC and to 0.06 arcsec with a PI controller. These results show that the control system can guarantee that the optical axis can be maintained in an ideal position in order to achieve high-resolution imaging.

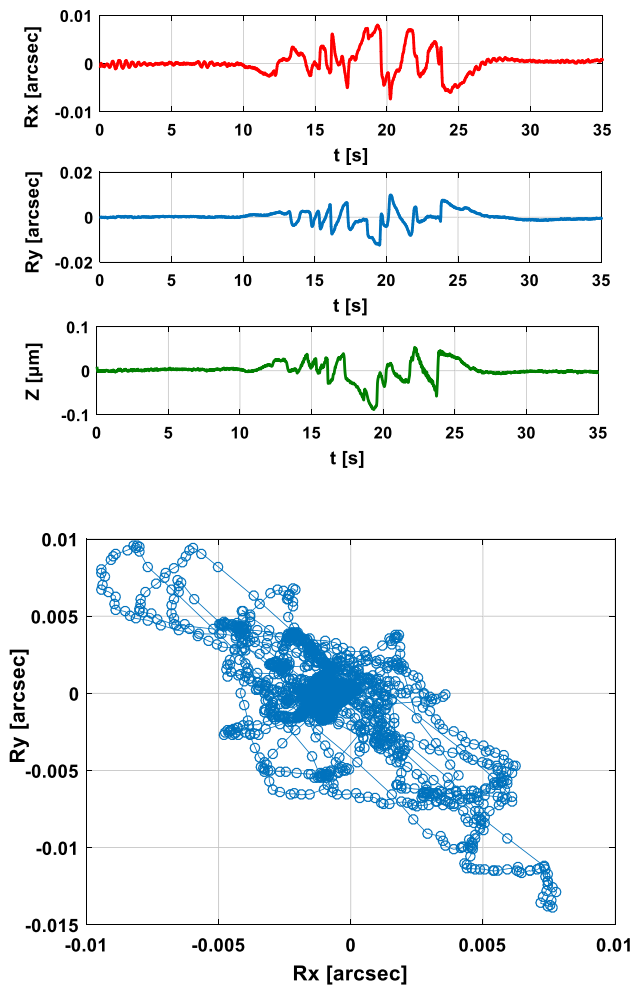


Fig. 13 POPM characteristics of the 1.2 m large telescope whose elevation axis moves at the controlled vibrational speed when ADRC and SMC controllers are used: **a** Inclinations in the x-direction and the y-direction (R_x and R_y respectively) and the shift in the z-direction (Z) and **b** two-dimensional plot of R_y as a function of R_x is presented

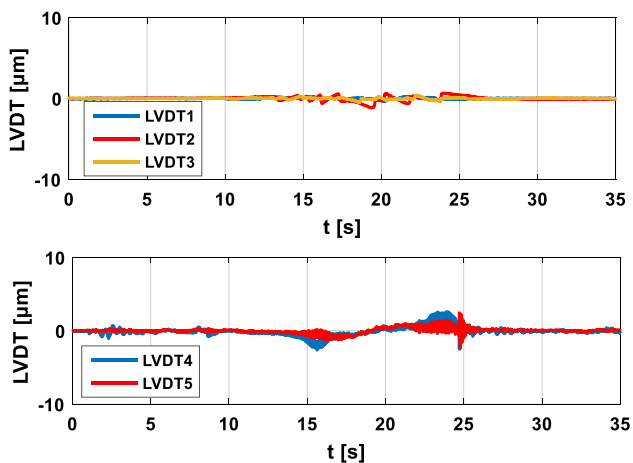


Fig. 14 LVDT errors of the five partitions when the elevation changes at different controlled speeds

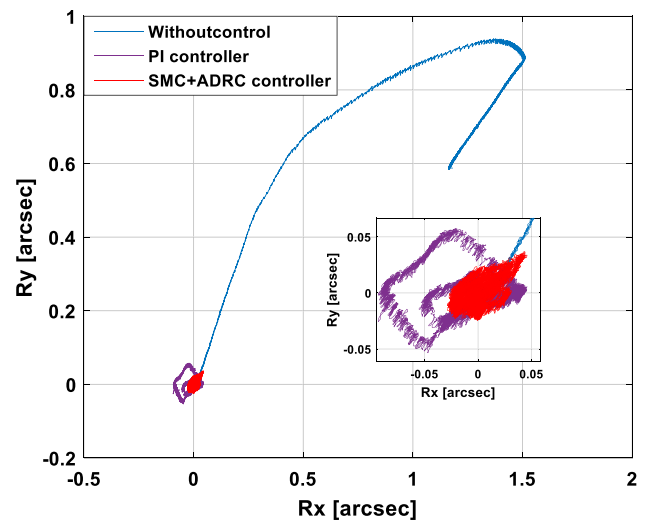


Fig. 15 Comparison of the POPM two-dimensional displacements using SMC and ADRC controllers, a PI controller, and no controller

Acknowledgements This research was supported by the National Natural Science Foundation of China (No. 11973041, No. 11803035).

References

1. E.D. Knoh, C. Oberkochen, VLT Primary Support system. *SPIE* **2199**(277), 271–283 (1998)
2. P.Y. Bely, *The Design and Construction of Large Optical Telescopes[M]* (Springer, New York, 2003), pp. 311–344
3. J.Q. Chen, *Principles of Astronomical Telescope Design [M]* (Science and Technology Press, Beijing, 2003)
4. J.L. Wang, X.Y. Liu, Concept and development of smart optics[J]. *Chin. J. Opt.* **6**(4), 437–448 (2013)
5. X.X. Wu, J.F. Li, S.M. Song et al., Active support system for 4 m SiC lightweight primary Mirror [J]. *Opt. Precis. Eng.* **22**(9), 2451–2457 (2014)
6. P. Schipani, D. Magrin, L. Noethe et al., The active optics system of the VST: concepts and results [C]. *Int. Soc. Opt. Photonics* (2012). <https://doi.org/10.1117/12.925493>
7. J.E. Kimbrell, G. David, AEOS 3.67m Telescope Primary Mirror Active Control System, Part of the SPIE Conference on Advanced Technology Optical/IR Telescopes VI Kona, Hawaii March, vol. 3352, issue 6, pp. 400–411 (1998)
8. C. Molfese, P. Schipani, M. Capaccioli, VST primary mirror active optics electronics. *SPIE* **7019**, 1–10 (2008)
9. P. Schipani, L. Marty, F. Perrotta, The primary mirror control software for VST. *SPIE* **7740**, 1–9 (2010)
10. J.F. Maclean, Gemini primary mirror control system: design, implementation and experience. *SPIE* **2034**, 235–247 (2010)
11. L. Stepp, E. Huang, M. Cho, Gemini primary mirror support system. In *Advanced Technology Optical Telescopes V*, SPIE, vol. 2199, pp. 223–238 (2011)
12. L. Shao, X.X. Wu, F. Yang, Improvement on hydraulic whiffle-tree support system for SiC lightweight primary mirror. *Laser Infrared Eng.* **43**(11), 3820–3824 (2014)
13. J. Antebi, D. Dusenberry, A.A. Liepins, Conversion of the MMT to a 6.5 m telescope the optics support structure [J]. *SPIE* **1303**, 148–161 (1990)

14. L. Fan, J.X. Zhang, L. Shao, Axial support for large aperture primary mirror based on hydraulic Whiffle tree. *Laser Infrared Eng.* **42**(8), 2126–2131 (2013)
15. X. Peng, G. Gong, H. Yang et al., Novel electro-hydraulic position control system for primary Mirror supporting system [J]. *Adv. Mech. Eng.* (2016). <https://doi.org/10.1177/1687814016647946>
16. L.X. Quan, *Research on the Bag Accymulator's Basic Theory and Experiment Based on Pipaline Effect [D]* (Yanshan University, Qinhuangdao, 2005)
17. Y.T. Deng, J.L. Wang, H.W. Li, Speed control of PMSM with sliding mode disturbance observer, in *Mechatronics and Automation (ICMA)*, pp. 2209–2214 (2018)

Publisher's Note Springer Nature remains neutral with regard to jurisdictional claims in published maps and institutional affiliations.